Detailed study of NBTI characterization in 40-nm CMOS process using comprehensive models*

Yan Zeng(曾严)[1], Xiao-Jin Li(李小进)[1,†], Jian Qing(卿健)[1], Ya-Bin Sun(孙亚宾)[1,‡], Yan-Ling Shi(石艳玲)[1], Ao Guo(郭奥)[2], and Shao-Jian Hu(胡少坚)[2]

[1] *Shanghai Key Laboratory of Multidimensional Information Processing and Department of Electrical Engineering, East China Normal University, Shanghai* 200241, *China*

[2] *Shanghai Integrated Circuit Research & Development Center, Shanghai* 201203, *China*

(Received 4 June 2017; revised manuscript received 26 June 2017; published online 20 August 2017)

The impact of negative bias temperature instability (NBTI) can be ascribed to three mutually uncorrelated factors, including hole trapping by pre-existing traps ($\Delta V_{\rm HT}$) in gate insulator, generated traps ($\Delta V_{\rm OT}$) in bulk insulator, and interface trap generation ($\Delta V_{\rm IT}$). In this paper, we have experimentally investigated the NBTI characteristic for a 40-nm complementary metal–oxide semiconductor (CMOS) process. The power-law time dependence, temperature activation, and field acceleration have also been explored based on the physical reaction–diffusion model. Moreover, the end-of-life of stressed device dependent on the variation of stress field and temperature have been evaluated. With the consideration of locking effect, the recovery characteristics have been modelled and discussed.

Keywords: negative bias temperature instability (NBTI), reaction diffusion (RD), interface trap, H_2 locking effect

PACS: 85.30.De, 77.55.df, 66.30.J– **DOI:** 10.1088/1674-1056/26/10/108503

1. Introduction

Negative bias temperature instability (NBTI) has become one of the most critical reliability issues with the CMOS transistor scaling down.[1] It triggers the degradation in device parameters such as threshold voltage ($\Delta V_{\rm T}$), linear or saturation drain currents ($\Delta I_{\rm ds}$), transconductance, subthreshold, and thus deteriorates the performance of circuits and systems over time.[2–4]

The physical mechanisms of NBTI have been fully studied and then several comprehensive models have been proposed.[5–8] The NBTI effect can be attributed to three mutually uncorrelated components. They are the interface trap generation ($\Delta N_{\rm IT}$), the hole trapping in pre-existing defects ($\Delta N_{\rm HT}$), and the oxide bulk trap generation ($\Delta N_{\rm OT}$). $\Delta N_{\rm IT}$ is explained by the double interface reaction–diffusion (RD) model.[6,8] $\Delta N_{\rm HT}$ is thought to be a fast component,[8–10] and it can be described by the two-energy-well model.[8,11] $\Delta N_{\rm OT}$ in SiON bulk is strongly dependent on voltage drop across SiON interlayer (IL) and it is negligible for HKMG devices and low field scenarios.[6] During the stress phase, $\Delta N_{\rm HT}$ may fully saturate within several seconds, while $\Delta N_{\rm IT}$ and $\Delta N_{\rm OT}$ manifest themselves as power-law ramping. During the recovery, a part of the interface traps will be annealed by fast electron capturing in several seconds, and followed by the slow recovery of the remaining RD generated traps.[6,12] The slow recovery of NBTI is driven by the back diffused hydrogen molecules (H_2). However, the locking effect cannot be ignored, some of the released hydrogen (H) species during the stress can be trapped and these H species are considered to be locked and will not be involved during recovery.[6]

In this paper, the H_2 locking effect has been involved in characterizing the NBTI effect for a 40-nm CMOS process. The NBTI effect of 40-nm CMOS process under different stress voltages ($V_{\rm G_STR}$) and temperatures (T) have been experimentally studied, then the time exponent (n), activation energy ($E_{\rm A}$), and field acceleration ($\Gamma_{\rm E}$) have been thoroughly investigated. Moreover, the long-term recovery of NBTI effect has been described by the comprehensive models.

2. Experiment and devices

In order to distinguish the $\Delta N_{\rm OT}$ contribution from NBTI, the thick oxide ($t_{\rm ox} = 2.43$ nm) p-MOSFETs ($W/L =$ 9 μm/9 μm) have been chosen to sustain the higher stress voltages ($V_{\rm G_STR} = 1.8$ V and 2.3 V). Besides, lower voltages ($V_{\rm G_STR} = 1.1$ V, 1.3 V, and 1.5 V) have been applied to the other set of p-MOSFETs ($W/L = 1$ μm/1 μm) with thinner oxide ($t_{\rm ox} = 1.75$ nm). The different temperatures ($T = 125$ °C and 85 °C) have been applied, and both the stress and recovery last for 10^4 s. The initial threshold voltage ($V_{\rm T0}$) of each p-MOSFET has been extracted using the

*Project supported by the National Natural Science Foundation of China (Grant Nos. 61574056 and 61204038), the Natural Science Funds of Shanghai, China (Grant No. 14ZR1412000), the Fund from the Science and Technology Commission of Shanghai Municipality (Grant No. 14DZ2260800), and Shanghai Sailing Program (Grant No. 17YF1404700).

†Corresponding author. E-mail: xjli@ee.ecnu.edu.cn

‡Corresponding author. E-mail: ybsun@ee.ecnu.edu.cn

© 2017 Chinese Physical Society and IOP Publishing Ltd

constant current method. The drain-to-source voltage (V_{ds}) is kept to 50 mV and gate-to-source voltage (V_{gs}) increases until I_{ds} reaches $40 \times W/L$ (nA), then V_{T0} can be obtained by V_{gs}. To measure the drain current shift (ΔI_{ds}) caused by the NBTI, the MSM (measure-stress-measure) method has been adopted. Given the fresh drain current I_{ds0}, ΔI_{ds} can be transformed to ΔV_{th} by[13]

$$\Delta V_T = \left| \frac{\Delta I_{ds}}{I_{ds0}} \right| \cdot (V_{G_STR} - V_{T0}). \quad (1)$$

3. Long-term NBTI degradation

3.1. Degradation characteristic

As mentioned before, NBTI degradation is composed of three mutually uncorrelated underlying components ΔN_{IT}, ΔN_{HT}, and ΔN_{OT}. Time evolution of these three components can be expressed as the analytical equations as shown in Table 1.[7,14,15] ΔN_{IT} and ΔN_{HT} are dependent on identical electrical field (E_{ox}) and Arrhenius T activation. The activation energy for ΔN_{IT} includes the forward breaking (E_{AKF}), the reverse annealing (E_{AKR}) of Si–H bonds, and the H_2 diffusion (E_{ADH2}).[14] Time evolution of ΔN_{OT} has a stretched exponential form with Arrhenius T activation E_{AOT} and power-low voltage acceleration factor Γ_{OT}.[15] Note, the fitting parameters β_{OT} and η are also listed in Table 1. The interface trap generation ΔN_{IT} can be described by the double interface RD model.[8,9] The first interface refers to the Si/SiO_2 interface and the second involves the SiO_2/poly gate interface.

Table 1. NBTI models during stress phase.

Calculation: NBTI degradation in stress
$\Delta V_T = \frac{q}{C_{ox}} \times (\Delta N_{IT} + \Delta N_{HT} + \Delta N_{OT})$
$\Delta N_{IT} = A E_{ox} e^{(\Gamma_{IT} E_{ox})} \exp\left(-\frac{E_{AIT}}{kT}\right) t^{1/6}$; $E_{ox} = (V_G - V_{T0} - \Delta V_T)/t_{ox}$ $E_{AIT} = \frac{2}{3}(E_{AKF} - E_{AKR}) + \frac{E_{ADH2}}{6}$
$\Delta N_{HT} = B E_{ox} e^{\Gamma_{HT} E_{ox}} \exp\left(-\frac{E_{AHT}}{kT}\right)$
$\Delta N_{OT} = C(1 - e^{(-(t/w)^{\beta_{OT}})})$; $w = \eta (V_G - V_{T0} - \Delta V_T)^{-\Gamma_{OT}/\beta_{OT}} \exp\left(\frac{E_{AOT}}{kT\beta_{OT}}\right)$
A, B, C, $\Gamma_{IT} (= \Gamma_{HT})$ and E_{AKF} are fitting parameters
$E_{AKR} = 0.2$ eV, $E_{ADH2} = 0.58$ eV, $E_{AHT} = 0.052$ eV, $E_{AOT} = 0.16$ eV, $\beta_{OT} = 0.33$, $\Gamma_{OT} = 10$, $\eta = 5 \times 10^{12}$

The X–H bonds are mainly located at the Si/SiO_2 interface, where X may be silicon, nitrogen, oxygen, or different oxygen vacancy-related defects. During the NBTI stress, the holes in the inversion layer tunnel into the interface and get captured in Si–H bonds. The corresponding covalent bonds get weakened and can be easily broken by the thermal process.[8] Then, the broken Si–H bonds release H atoms that diffuse towards the poly gate and react with X–H to form H_2 molecules. The diffusion of H_2 determines the time evolution of ΔN_{IT} for a long stress time (t_{str}), and shows a power-law time dependence with an exponent of 1/6, as shown in Table 1.

Figure 1 compares the time evolution of the measured data and the model calculation for different devices. The total degradation is divided into ΔN_{IT}, ΔN_{HT}, and ΔN_{OT}. Figures 1(a) and 1(b) show the degradation of 9 μm×9 μm device under 1.8 V and 2.3 V, (c) and (d) show 1 μm×1 μm device under 1.1 V and 1.3 V, respectively. These thinner devices cannot survive in high V_{G_STR}, and the degradation under low voltage at $T = 85$ °C seems pretty small. Therefore, the higher temperature up to 125 °C has been used to accelerate the degradation. Then, similar degradation for two different devices has been achieved. ΔN_{HT} gets saturated and keeps constant after several seconds. When the stress voltage lower than 1.8 V is applied, it is believed that ΔN_{IT} plays a dominant role in the NBTI degradation, shown in panels (a), (c), and (d). ΔN_{OT} can be ignored for $V_{G_STR} = 1.1$ V and 1.3 V, it is believed that low oxide field is not enough to trigger the oxide bulk trap generation. Whereas, the contribution from ΔN_{OT} gradually dominates the degradation when the V_{G_STR} continues increasing. ΔN_{OT} is identified to be due to impact ionization and hot-hole generation in the substrate, which is triggered by hot electron injection from the gate cathode. Though ΔN_{IT} is mainly responsible for NBTI for a vast majority of cases, ΔN_{OT} dominates the overall degradation for stress at high V_{G_STR}.[16] Both ΔN_{OT} and ΔN_{IT} manifest themselves as a power-law function of time. When V_{G_STR} is elevated up to 1.8 V, the contribution from ΔN_{OT} is about 16% of the total degradation at 10^4 s. Given $V_{G_STR} = 2.3$ V, the relative contribution is up to 58%. In contrast, the contribution from ΔN_{IT} continues to decrease with V_{G_STR} increasing, giving 89%@ $V_{G_STR} = 1.3$ V, 73%@$V_{G_STR} = 1.8$ V, and 58%@$V_{G_STR} = 2.3$ V. Figure 2 also shows a good agreement between the measured data and the calculation for other devices and stress conditions. Note that only the total degradations have been given, here the individuals of ΔN_{OT}, ΔN_{HT}, and ΔN_{IT} are not shown.

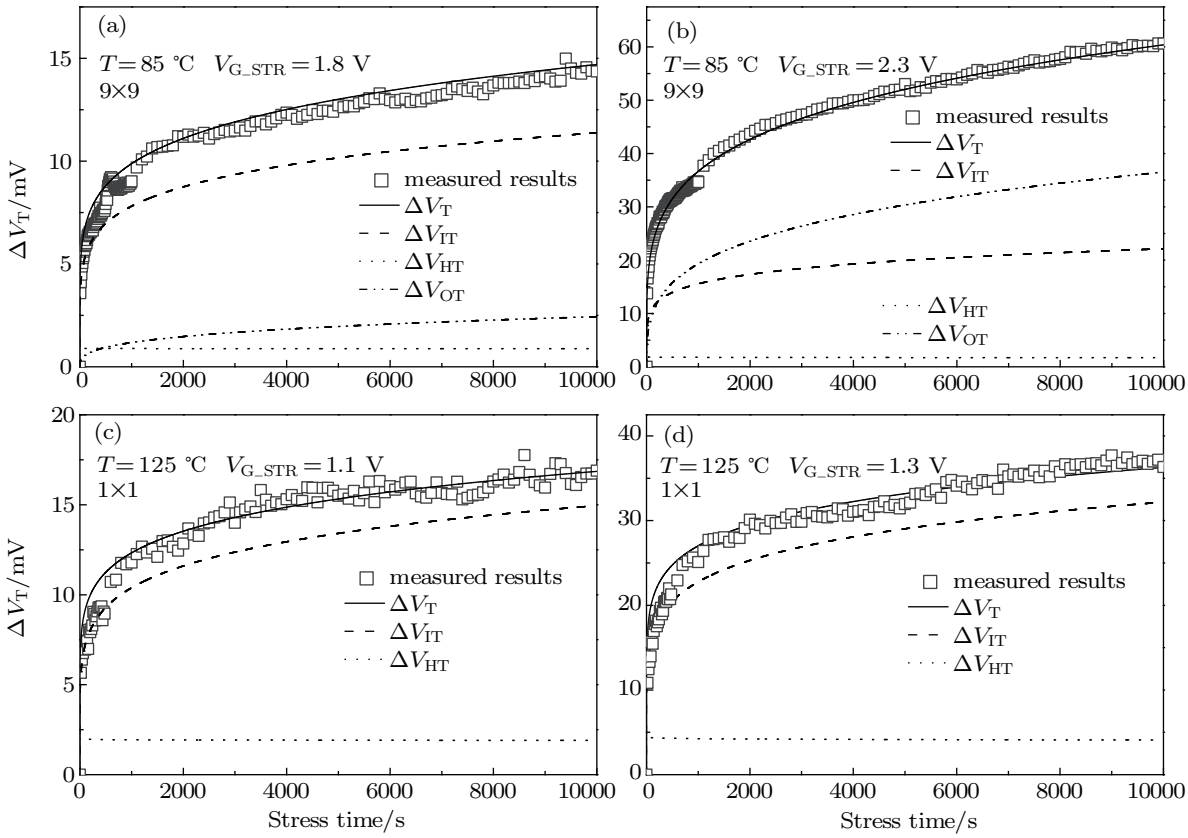


Fig. 1. Experimental ΔV_{T}, the model calculation and the underlying components under different stress conditions.

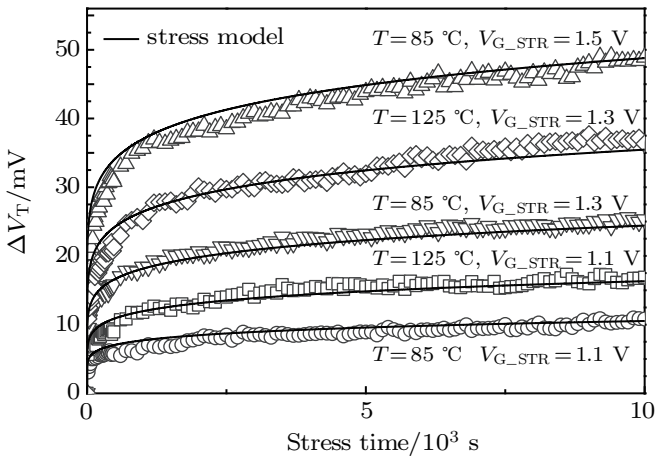


Fig. 2. Time evolution of ΔV_{T} and the model calculation under different stress conditions, the extracted parameters: $(q/C_{\mathrm{ox}})\cdot A = 0.96$ (1/cm·s$^{1/6}$), $(q/C_{\mathrm{ox}})\cdot B = 0.141$ (1/cm), $C = 0$ (ΔN_{OT} is negligible at low voltage), $\Gamma = 0.54$ (cm/MV), $E_{\mathrm{AKF}} = 0.207$ (eV).

In order to investigate the time evolution of each subcomponent, the relative contribution of each one under different $V_{\mathrm{G_STR}}$, T, and t_{str} have been analyzed. Figures 3(a), 3(b), and 3(c) show the relative contribution under different $V_{\mathrm{G_STR}}$ at 10^4's. As $V_{\mathrm{G_STR}}$ increases the relative contribution of ΔN_{OT} goes up, whereas ΔN_{IT} have the opposite tendency. Their cross points locate at 2.4 V, 2.15 V, and 2.05 V for 25 °C, 85 °C, and 125 °C, respectively, and they may decrease as the temperature is elevated. Figures 3(d), 3(e), and 3(f) show the relative contributions of ΔN_{IT}, ΔN_{HT}, and ΔN_{OT} changing with $V_{\mathrm{G_STR}}$ under different stress times but at the same temperature (85 °C). Longer t_{str}, faster ΔN_{IT} descending. The longest t_{str} leads to the largest ΔN_{IT} at small $V_{\mathrm{G_STR}}$, giving 95%. With $V_{\mathrm{G_STR}}$ increasing from 1.3 V to 2.3 V, the longest t_{str} drops to less than 30%. The root cause is that the generation rate of ΔN_{OT} overwhelms ΔN_{IT} with $V_{\mathrm{G_STR}}$ ramping, ΔN_{OT} shows a stronger bias dependence than that of ΔN_{IT}, see Fig. 3(f). Since ΔN_{HT} is easy to saturate it plays a more important role at smaller t_{str}, as shown in Fig. 3(e).

The device lifetime τ is defined as the time when the device drain current reaches 10% relative degradation. Figure 4 shows the relationship between the device lifetime and the initial oxide field ($E_{\mathrm{ox}} = (V_{\mathrm{G_STR}} - V_{\mathrm{T0}})/t_{\mathrm{ox}}$) based on our extracted parameters. It is suggested that $\log(\tau)$ is a linear function of E_{ox}, larger E_{ox} and/or higher T lead to shorter lifetime.

3.2. Analysis of NBTI parameters

To better understand the NBTI features in 40-nm process, time exponent n, Arrhenius temperature activation E_{A}, and power-law oxide field acceleration Γ_{E} have been explored. The experimental data are from the p-MOSFETs with thin gate insulator and low stress voltage, thus ΔN_{IT} dominates the long-term degradation in which ΔN_{OT} is excluded.

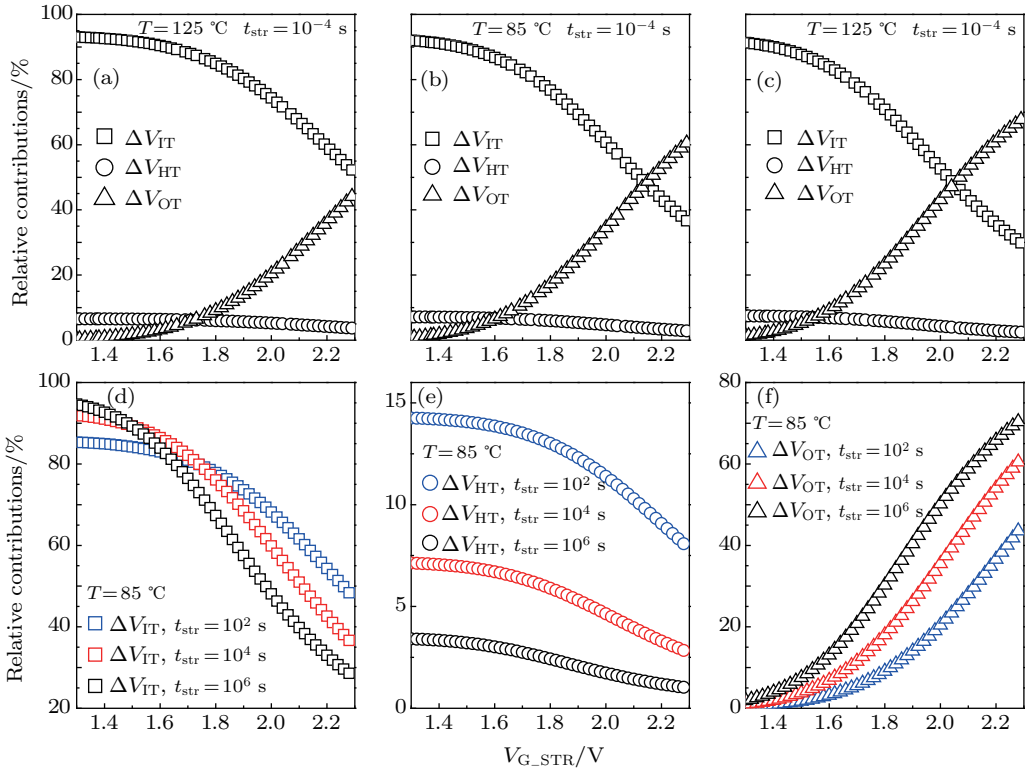


Fig. 3. (color online) (a)–(c) Relative contributions from ΔN_{IT}, ΔN_{HT}, and ΔN_{OT} versus V_{G_STR} under different T at $t_{str} = 10^4$ s, (d)–(f) V_{G_STR} dependence of the relative contributions from each subcomponents for different t_{str} at given $T = 85$ °C.

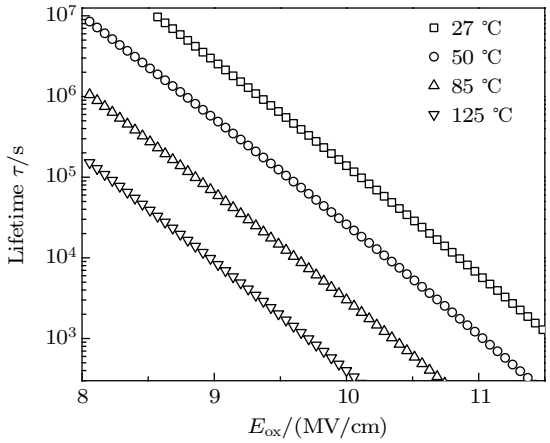


Fig. 4. Lifetime under different E_{ox} and T based on the extracted parameters.

3.2.1. Time exponent

The power-law time exponent is of vital importance as it determines the extrapolation from the measured data to the lifetime of a device. Across a large variety of devices and circuits, n is observed to be a universal parameter which approximates 1/6.[17] It is found that measured data of ΔV_T versus t_{str} are parallel to each other for different E_{ox} and T when plotted in log-log scale, and n can be calculated from ΔV_T time evolution by linear regression in $t_{str} = 100 \sim 10^4$ s. Figure 5 shows the relationship between n and E_{ox}, and it also implies $n \approx 1/6$, which is consistent with the physical explanation. Note that, in this extraction, ΔV_{HT} $(= q^* \Delta N_{HT}/C_{ox})$ saturates, ΔV_{OT} is excluded due to low V_{G_STR}, and ΔV_{IT} $(= q^* \Delta N_{IT}/C_{ox})$ plays a dominant role.

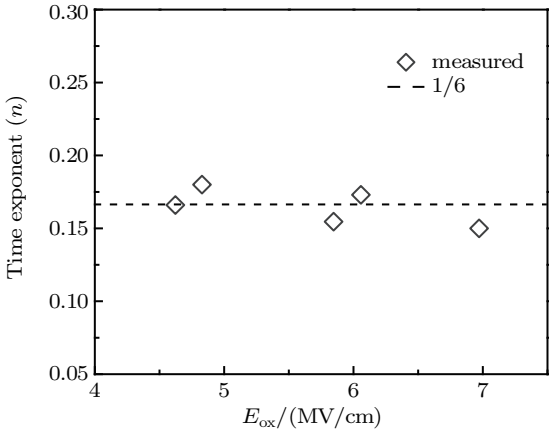


Fig. 5. Extracted time exponent $n \sim E_{ox}$.

3.2.2. Temperature activation

Figure 6 shows our measured ΔV_T and the reported $\Delta I_{ds}/I_{ds0}$[18] as two functions of stress temperature T for a given t_{str}. NBTI degradation has a linear relationship with $1/kT$ in semi-log scale, where k is the Boltzmann constant. As equation (1) shows, ΔV_T is proportional to $\Delta I_{ds}/I_{ds0}$ and therefore, E_A can be extracted. The extracted E_A (0.089 eV) from our experimental data is close to 0.096 eV which is reported.[18] Hole trapping subcomponent ΔV_{HT} (0.052 eV) has a lower activation energy compared with that of ΔV_{IT}, and thus ΔV_{HT} reduces the overall equivalent E_A. However,

because ΔV_{IT} dominates the long-term degradation at lower V_{G_STR} (< 1.8 V), the overall E_A is determined by ΔV_{IT}. According to RD theory, ΔV_{IT} time evolution is controlled by molecule H_2 diffusion and shows an activation of $E_{ADH2} \sim 0.6$ eV.[15] Since Si–H bond dissociation and passivation are similarly activated, E_{AKF} is approximately equal to E_{AKR}. The temperature activation at given t_{str} would be described as $E_{AIT} \approx E_{ADH2}/6 \approx 0.1$ eV, seen in Table 1. Consider the contribution of ΔV_{HT}, E_A of overall ΔV_T will be close to but lower than 0.1 eV, which is consistent with the discussion above, giving the extracted E_A of 0.089 eV.

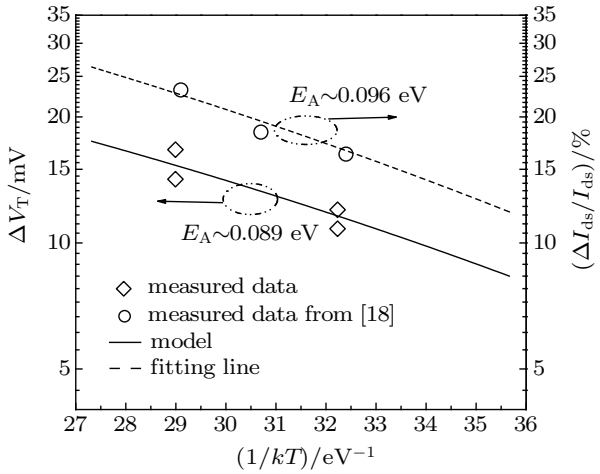


Fig. 6. Measured ΔV_T and $\Delta I_{ds}/I_{ds0}$ as a function of T at given t_{str}.

3.2.3. Field acceleration

The oxide field dependence of ΔV_{IT} and ΔV_{HT} originates from holes in the inversion layer tunneling to Si–H bonds and pre-existing traps.[8] ΔV_{IT} and ΔV_{HT} are proportional to the term of $E_{ox} \cdot \exp(\Gamma \cdot E_{ox})$. Assume ΔN_{IT} and ΔN_{HT} have the same field acceleration factor, giving $\Gamma_{IT} = \Gamma_{HT}$, for simplicity and generality, the field acceleration factor Γ_E of overall degradation has been extracted. Figure 7 shows that the NBTI degradation under different temperatures have the identical Γ_E, different temperatures have the similar $\Gamma_E \sim 3.55$.

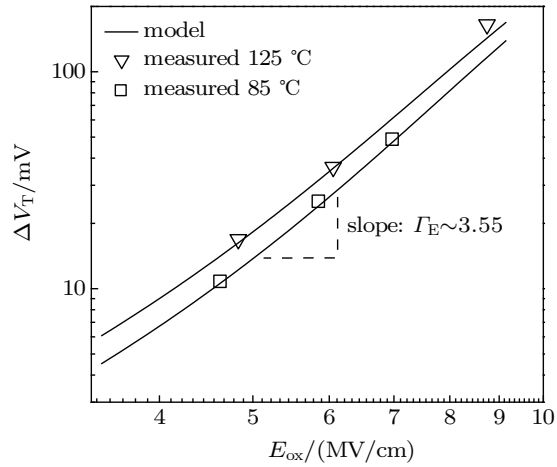


Fig. 7. Measured ΔV_T and model prediction at $t_{str} = 10^4$ s for varying E_{ox}.

4. NBTI recovery

In the double interface RD model,[6,8,9] the slow recovery is described as a H_2 molecule diffusing back from poly to the gate insulator and reacting with the broken X^- to form X–H bonds. The resultant H atoms diffuse towards the interface of SiO_2/Si to form Si–H bonds. The X-defects are randomly distributed in the gate insulator and H_2 molecule needs to hop around until it is captured. With the passivation of broken X^- continuing, the probability of H_2 finding an available defect decreases over time and the hopping of H_2 molecule would last longer. This physical process can be characterized by slowing down H_2 diffusivity over time.[6,11] Furthermore, some released H species may be locked in traps or get out of the system and thus a fraction of degradation remains permanent.[6,19]

During NBTI recovery phase, hole trapping in ΔN_{HT} and ΔN_{OT} can rapidly recover within several seconds.[6,20] A fraction of ΔN_{IT} below the Fermi level may capture electrons, behaving as a fast recovery. On the other hand, the remaining broken bonds above the Femi level may be passivated by the back-diffused H_2 and H. The slow recovery of NBTI degradation is mainly contributed by the passivation of interface defects with back diffusion of H_2.[21] In general, the total recovery consists of three uncorrelated components, they are 1) fast recovery of ΔV_{HT} and ΔV_{OT}, 2) fast electron capture by partial ΔV_{IT} (ΔV_{IT1}), and 3) slow recovery of the remaining ΔV_{IT} (ΔV_{IT2}).[6]

Table 2. NBTI model for recovery.

Calculation: NBTI degradation in recovery
$\Delta V_T = \Delta V_{IT1} + \Delta V_{IT2} + \Delta V_{HT}$
$\Delta V_{IT1}(t) = \Delta V_{IT0} \cdot F_{FAST} \cdot exp\left[-\left(\frac{t}{\tau_{EC}}\right)^{\beta_{EC}}\right]$
$\Delta V_{IT2}(t) = \Delta V_{IT0}(1-F_{FAST})(1-\alpha)\left(1-\sqrt{\frac{\xi t}{t_{str}+t}}\right) + \Delta V_{IT0}(1-F_{FAST})\alpha$
$\Delta V_{HT}(t) = \Delta V_{HT0} \cdot \exp\left[-\left(\frac{t}{\tau_{REC}}\right)^{\beta_{REC}}\right]$
τ_{EC}, β_{EC}, τ_{REC}, β_{REC}, ξ, F_{FAST}, and α are fitting parameters

In this work, an analytical model derived by the RD theory considering H_2 locking effect has been adopted to describe the time evolution of ΔV_{IT2}, as shown in Table 2. ΔV_{IT0} and ΔV_{HT0} are the initial degradations before recovery and can be calculated by the model in Table 1. F_{FAST} is introduced to describe the fraction of ΔN_{IT} which rapidly recovers, the term of $\Delta V_{IT0} \cdot F_{FAST}$ is the fast recovery, and $\Delta V_{IT0} \cdot (1 - F_{FAST})$ is the slow counterpart. Furthermore, the factor α is also introduced to account for the unrecovered ΔV_{IT2}. When the recovery time is less than the stress, giving $t_{rec} < t_{str}$, the factor ξ manifests itself as a constant.[22] The analytical solution of the

fast recovery components ΔV_{IT1} and ΔV_{HT} have been listed in Table 2.[6,23] Note that the contribution from ΔV_{OT} has been ignored because the applied V_{G_STR} is not enough to trigger the oxide bulk trap generation.

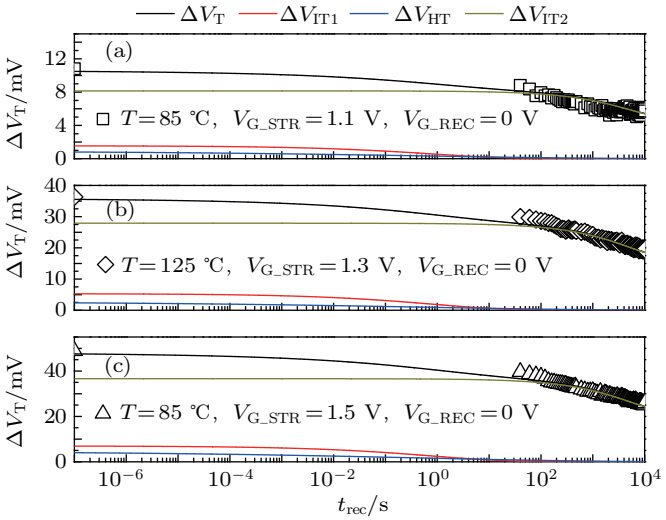


Fig. 8. (color online) Time evolution of measured ΔV_T (symbols) under different conditions for NBTI recovery. Overall model prediction for ΔV_T and underlying ΔV_{IT1}, ΔV_{IT2}, and ΔV_{HT} subcomponents are also shown.

Figure 8 shows the time evolution of measured ΔV_T after NBTI stress for different V_{G_STR} and temperatures. The calculated ΔV_T and its underlying subcomponents have been extracted. ΔV_{IT1} and ΔV_{HT} fully recover within several seconds and ΔV_{IT2} determines the long-term recovery process. Note, during the recovery the stress voltage is withdrawn and the temperature is kept. The relative contributions of ΔV_{IT1}, ΔV_{HT}, and ΔV_{IT2} are different as shown in Fig. 9. When the stress time is smaller, the contribution from ΔV_{HT} will be larger and the overall degradation will recover faster. The shorter the stress time, the larger the relative ΔV_{HT}. Given t_{str} as 100 s, 10^4 s, and 10^6 s, the contribution of ΔV_{IT2} in the remaining overall degradation achieve 95% at t_{rec} of 800 s, 40 s, and 8 s, respectively. Since the difference between ΔV_{IT2} and ΔV_T is smaller than 5%, the slow recovery due to ΔV_{IT2} begins to dominate the long-term degradation at 796 s, 38 s, and 8 s. In general, ΔV_{IT} dominates the overall degradation and then slows the recovery.

Figure 10 shows that the time evolutions of measured ΔV_T adhere to the model prediction well under different stress conditions. It is found that about 44% of the degradation accumulated during the stress recovers at the time $t_{rec} = 5 \times 10^3$ s across different conditions. Given $T = 85$ °C, the recovered percentages are 43.38%@$V_{G_STR} = 1.1$ V, 44.3%@$V_{G_STR} = 1.3$ V, and 43.8%@$V_{G_STR} = 1.5$ V at $t_{rec} = 5 \times 10^3$ s, respectively. When $T = 125$ °C, $V_{G_STR} = 1.1$ V has a 45.2% recovery proportion at $t_{rec} = 5 \times 10^3$ s, while $V_{G_STR} = 1.3$ V has 43.0%.

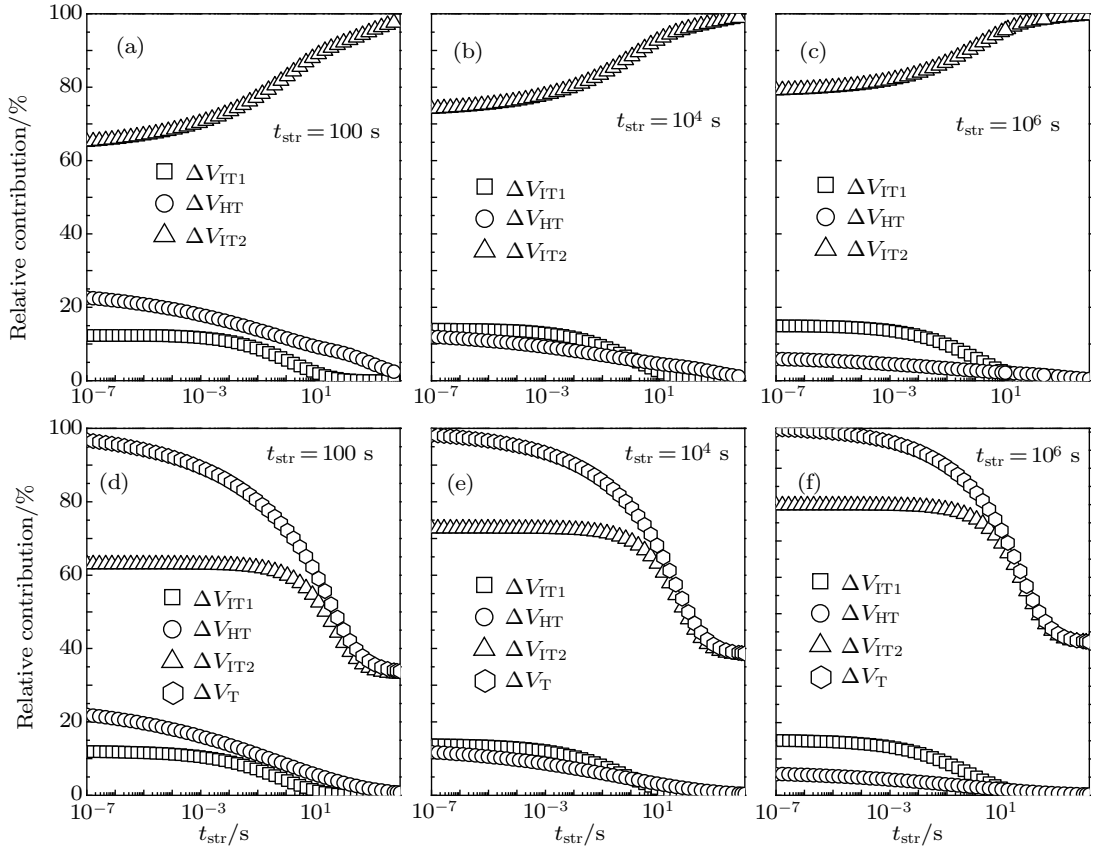


Fig. 9. (a)–(c) Relative contributions of the remaining ΔV_{IT1}, ΔV_{HT}, and ΔV_{IT2} to the overall degradation, (d)–(f) relative contribution of the remaining ΔV_T, ΔV_{IT1}, ΔV_{HT}, and ΔV_{IT2} to their initial degradation ΔV_{T0}, respectively, for different NBTI stress times at $T = 85$ °C, $V_{G_STR} = 1.5$ V, and $V_{G_REC} = 0$ V.

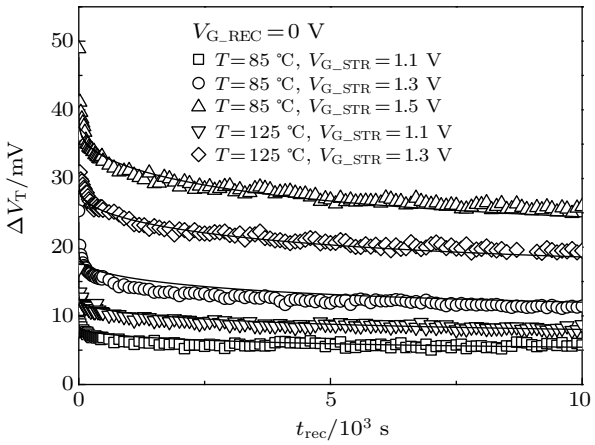


Fig. 10. The experimental ΔV_T, and analytical model prediction under different conditions, the parameters of the analytical model are given as $(1-F_{FAST})(1-\alpha)\xi^{1/2} = 0.4$, and $F_{FAST} = 0.16$, $\tau_{EC} = 0.8$, $\beta_{EC} = 031$, $\tau_{REC} = 0.5$, $\beta_{REC} = 0.128$.

5. Conclusions

With the comprehensive stress/recovery models, the long-term NBTI degradation in 40-nm process has been thoroughly studied. Based on the experimental data, the relative contributions from ΔN_{IT}, ΔN_{HT}, and ΔN_{OT} have been analyzed. Time exponent, Arrhenius temperature activation, and power-law oxide field acceleration have been extracted, given as $n \sim 1/6$, $E_A \sim 0.089$ eV, and $\Gamma_E \sim 3.55$. During the NBTI recovery, the characteristics of each subcomponent have also been described and discussed. It can be concluded that the NBTI characteristic of 40-nm process can be well described by the comprehensive models and our extracted model parameters.

References

[1] Tang H L, Xu B L, Zhuang Y Q, Zhang L and Li C 2016 *Acta Phys. Sin.* **65** 168502 (in Chinese)

[2] Krishnan A T, Reddy V, Chakravarthi S, Rodriguez J, John S and Krishnan S 2003 *IEEE International Electron Devices Meeting*, 8–10 December, 2003, p. 14.5.1

[3] Liu H X and Hao Y 2016 *Chin. Phys.* **16** 2111

[4] Cao Y R, Ma X H, Hao Y and Hu S G 2010 *Chin. Phys. B* **19** 047307

[5] Joshi K, Mukhopadhyay S, Goel N and Mahapatra S 2012 *IEEE International Reliability Physics Symposium*, 15–19 April, 2012, p. 5A.3.1

[6] Mahapatra S (ed.) 2016 *Fundamentals of Bias Temperature Instability in MOS Transistors* (New Delhi: Springer) pp. 209–263

[7] Goel N, Joshi K, Mukhopadhyay S, Nanaware N and Mahapatra S 2014 *Microelectron. Rel.* **54** 491

[8] Mahapatra S, Goel N, Desai S, Gupta S, Jose B, Mukhopadhyay S, Joshi K, Jain A, Islam A E and Alam M A 2013 *IEEE Trans. Electron Dev.* **60** 901

[9] Parihar N, Goel N, Chaudhary A and Mahapatra S 2016 *IEEE Trans. Electron Dev.* **63** 946

[10] Mahapatra S, Islam A, Deora S, Maheta V, Joshi K, Jain A and Alam M, 2011 *International Reliability Physics Symposium,* 10–14 April, 2011, p. 6A.3.1

[11] Desai S, Mukhopadhyay S, Goel N, Nanaware N, Jose B, Joshi K and Mahapatra S 2013 *IEEE International Reliability Physics Symposium*, 14–18 April, 2013, p. XT.2.1

[12] Yoshiki Y 2014 *Microelectron. Rel.* **54** 520

[13] Krishnan A T, Chancellor C, Chakravarthi S, Nicollian P E, Reddy V, Varghese A, Khamankar R B and Krishnan S 2005 *IEEE International Electron Devices Meeting Technical Digest*, 5–7 December, 2005, p. 691

[14] Joshi K, Mukhopadhyay S, Goel N, Nanware N and Mahapatra S 2014 *IEEE Trans. Electron Dev.* **61** 408

[15] Mahapatra S (ed.) 2016 *Fundamentals of Bias Temperature Instability in MOS Transistors* (New Delhi: Springer), pp. 127–179

[16] Mahapatra S, Kumar P B and Alam M A 2004 *IEEE Trans. Electron Dev.* **51** 1371

[17] Mahapatra S, Huard V, Kerber A, Reddy V, Kalpat S and Haggag A 2014 *IEEE International Reliability Physics Symposium Proceedings*, 1–5 June, 2014, p. 3B.1.1

[18] Nozomu K, Yasuhiro D and Nobuyuki W 2009 *Microelectron. Rel.* **49** 989

[19] Rangan S, Mielke N and Yeh E C C 2003 *IEEE International Electron Devices Meeting Technical Digest*, 8–10 December, 2003, p. 14.3.1

[20] Deora S, Maheta V, Islam A, Alam M, and Mahapatra S 2009 *IEEE Electron Dev. Lett.* **30** 978

[21] Cao Y R, Yang Y, Cao C, He W L, Zheng X F, Ma X H and Hao Y 2015 *Chin. Phys. B* **24** 097304

[22] Kumar S V, Kim C H, Sapatnekar S S 2009 *IEEE Trans. Dev. Mater. Rel.* **9** 537

[23] Goel N, Naphade T and Mahapatra S 2015 *IEEE International Reliability Physics Symposium*, 19–23 April, 2015, p. 4A.3.1